Materials and Design 199 (2021) 109417

Contents lists available at ScienceDirect

Materials and Design

journal homepage: www.elsevier.com/locate/matdes

Grain boundary oxide layers in NdFeB-based permanent magnets

A. Mazilkin [a,b], B.B. Straumal [a,b,c,*], S.G. Protasova [b], S. Gorji [a,d], A.B. Straumal [b,c], M. Katter [e], G. Schütz [f], B. Barezky [a]

[a] Karlsruhe Institute of Technology, Institute of Nanotechnology, Eggenstein-Leopoldshafen, Germany
[b] Institute of Solid State Physics and Chernogolovka Scientific Center of RAS, Chernogolovka, Russia
[c] National University of Science and Technology «MISIS», Moscow, Russia
[d] KIT-TUD-Joint Research Laboratory Nanomaterials, Technische Universität Darmstadt, Darmstadt, Germany
[e] Vacuumschmelze GmbH & Co. KG, 63412 Hanau, Germany
[f] Max-Planck Institute of Intelligent Systems, Stuttgart, Germany

HIGHLIGHTS

- It has been observed that $Nd_2Fe_{14}B$/$Nd_2Fe_{14}B$ GBs in the NdFeB-based alloys for permanent magnets can contain Nd_2O_3 oxide layers.
- It has been also shown that Nd_2O_3 oxide GB layers, similar to GBs with metallic Nd or intermetallic phases, can effectively ensure the magnetic isolation of $Nd_2Fe_{14}B$ grains from each other.
- Therefore, the GB oxide layers can be used for further development of NdFeB-based permanent magnets.

GRAPHICAL ABSTRACT

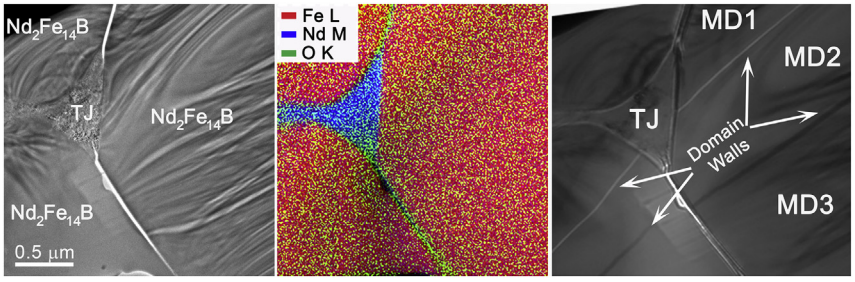

ARTICLE INFO

Article history:
Received 30 June 2020
Received in revised form 16 December 2020
Accepted 16 December 2020
Available online 22 December 2020

Keywords:
Permanent magnets
Coercivity
Nd-Fe-B alloys
Oxide layers
Grain boundaries
Thin layers

ABSTRACT

The microstructure of grain boundaries (GBs) in the commercial NdFeB-based alloy for permanent magnets has been studied. It is generally accepted that the unique hard magnetic properties of such alloys are controlled by the thin layers of a Nd-rich phase in $Nd_2Fe_{14}B$/$Nd_2Fe_{14}B$ GBs. These GB layers ensure the magnetic isolation of $Nd_2Fe_{14}B$ grains from each other. It is usually supposed that such GB layers contain metallic Nd or Nd-rich intermetallic compounds. However, the commercial NdFeB-based permanent magnets frequently contain a tangible amount of neodymium oxide Nd_2O_3 at the triple junctions between $Nd_2Fe_{14}B$ grains. The goal of this work was to check whether the $Nd_2Fe_{14}B$/$Nd_2Fe_{14}B$ GBs could also contain the thin layers of Nd_2O_3 oxide phase. Indeed, the screening with EELS-based elemental analysis permitted to observe that some of these Nd-rich layers in $Nd_2Fe_{14}B$/$Nd_2Fe_{14}B$ GBs contain not only neodymium, but also oxygen. More detailed analysis of such GBs with high-resolution transmission electron microscopy (HR TEM) showed these GB layers are crystalline and have the lattice of neodymium oxide Nd_2O_3. In turn, the Lorentz micro-magnetic contrast in TEM permitted to observe that the Nd-oxide GB layers prevent the migration of domain walls from one $Nd_2Fe_{14}B$ grain to another during remagnetization. This finding proves that the GB oxide layers, similar to those of metallic Nd or Nd-rich intermetallic compounds, can ensure the magnetic isolation between $Nd_2Fe_{14}B$ grains needed for high coercivity. Therefore, the GB oxide layers can be used for further development of NdFeB-based permanent magnets.

* Corresponding author at: Institute of Solid State Physics, Russian Academy of Sciences, Moscow district, Chernogolovka 142432, Russia.
E-mail address: straumal@issp.ac.ru (B.B. Straumal).

https://doi.org/10.1016/j.matdes.2020.109417

1. Introduction

Since their discovery in 1980-ies, Nd-Fe-B-based alloys remain the best ones among other permanent magnets [1–7]. They possess the highest magnetic energy product $(BH_c)_{max}$ (B being the saturation magnetization, and H_c being the coercivity). Their B value has almost reached its theoretical limit thanks to the favorable combination of magnetic characteristics (saturation magnetization, and uniaxial anisotropy constant) of $Nd_2Fe_{14}B$ intermetallic compound and careful alloying of the NdFeB-based permanent magnets. During this alloying, Nd is partially substituted by Pr and other rare-earth metals (REMs), and Fe is partially substituted by other transition metals (TMs) in the lattice of $Nd_2Fe_{14}B$ phase [4–7]. However, the coercivity is still far away from its possible maximum. H_c increases if the domain walls have a limited mobility, and cannot move from one $Nd_2Fe_{14}B$ grain to another when the external magnetic field changes its direction and value [4,5].

Usually, the Nd-rich phase in grain boundaries (GBs) is responsible for this "magnetic isolation" or decoupling of $Nd_2Fe_{14}B$ grains from each other [4–13]. For the best performance, the fraction of $Nd_2Fe_{14}B/Nd_2Fe_{14}B$ GBs covered by the Nd-rich phase has to be as high as possible. On the other hand, the total amount of Nd-rich phase has to be kept possibly low since the Nd-rich phase is non-ferromagnetic and, therefore, decreases the overall B value of a whole magnet. Usually, the Nd-rich phase in $Nd_2Fe_{14}B/Nd_2Fe_{14}B$ GBs and GB triple junctions (TJs) appears during the liquid-phase sintering of $Nd_2Fe_{14}B$ powder with REMs at about 1100 °C followed by a definite heat treatment [7,8,13]. It is generally believed nowadays that this Nd-rich phase is always formed by metallic Nd or several Nd-rich binary, ternary or multicomponent compounds consisted of REMs, TMs and boron [5,13].

However, the commercial NdFeB-based permanent magnets contain not only REMs, TMs and boron. During the production, some oxygen is always present in the protective atmosphere, and the easily oxidizing REMs form the oxides. The oxides are almost inevitable in commercial magnets. Large (from several to tens of μm) oxide particles in GB TJs are easily observed in the samples not only in our study (see Fig. 1) but also in most published works [13–20]. Unfortunately, only few authors have discussed the possible role of GB oxide layers in NdFeB-based permanent magnets [21]. Partially, it is because the experimental possibility for the reliable local measurements of oxygen content using electron energy loss spectroscopy (EELS) with simultaneous determination of oxide phase crystal structure by means of high-resolution TEM (HRTEM) is not always available. Recently, few studies were done where oxygen was detected in thin layers of Nd-rich GB phase by means of EELS technique [22,23].

The goal of this work is to reconsider the GB layers of Nd-rich phase in NdFeB-based permanent magnets by means of HRTEM and analytical TEM techniques, like EELS and energy filtered TEM (EFTEM), in combination with qualitative TEM magnetic imaging at zero field to address the following questions:

i. Can some Nd-rich layers in $Nd_2Fe_{14}B/Nd_2Fe_{14}B$ GBs indeed contain oxygen together with REMs?
ii. Can the Nd-oxide GB layers prevent the migration of domain walls from one $Nd_2Fe_{14}B$ grain to another and thus ensure the magnetic isolation (decoupling) between the grains (similar to GBs covered by metallic Nd or Nd-rich intermetallic compound)?

2. Experimental

The commercial NdFeB-based permanent magnet alloy delivered by Vacuumschmelze GmbH & Co. KG was studied. It contained (in wt%) 22.5 Nd, 10 Dy, <0.1 Pr, <0.1 Tb, 0.9 B, 1.0 Co, 0.1 Cu, 0.1 Al, 0.15 Ga, 0.4 O, 0.04C, balance Fe. This alloy was sintered at 1020 °C and then annealed at 800 and 500 °C consequently. It had a remanence of $B_r = 134$ A m^2/kg and coercivity of $H_c = 1.95$ T (measured at 20 °C) (Fig. 2).

Scanning electron microscopy (SEM) with EDX analysis was performed on a Zeiss Auriga 60 microscope equipped with EDAX Apollo EDX detector. For the sample imaging, the back-scattered electron (BSE) detector was used. The samples for SEM were prepared by grinding followed by polishing with water free diamond emulsions to prevent excessive oxidation of the sample surface.

NdFeB samples are hard magnets; to reduce the influence on the electron beam in the TEM, we used a focused ion beam (FIB) system to prepare a small sample for the TEM analysis. TEM lamellae were

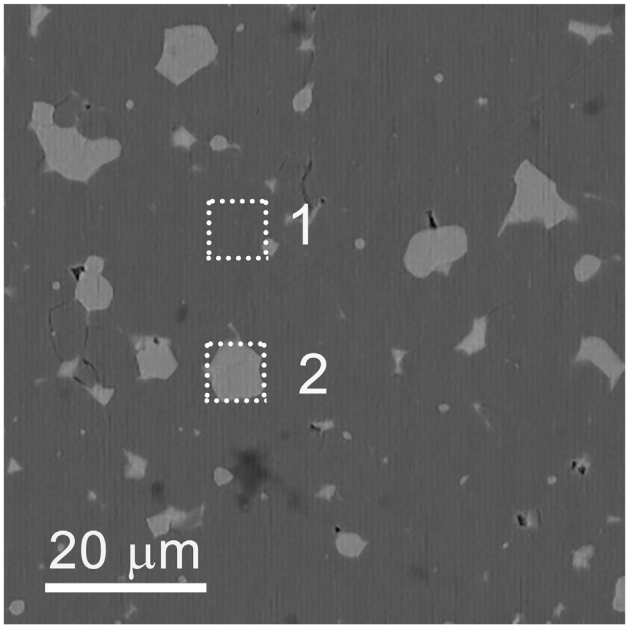

Fig. 1. BSE SEM micrograph of the studied NdFeB-based commercial alloy. The $Nd_2Fe_{14}B$ grains in the matrix appear dark grey. The brighter areas in TJs and along GBs are the phases with high Nd content. EDX elemental analysis (Table 1) was conducted for two sample areas, i.e. sample matrix (area 1) and GB TJ (area 2).

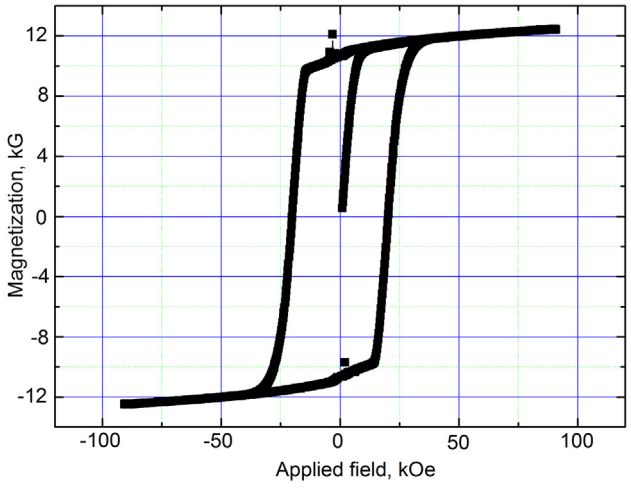

Fig. 2. Magnetization curve for studied alloys at 20 °C (in the direction of easy magnetization).

prepared using a FEI Strata dual-beam facility consequently at 30 and 2 kV. The low-voltage step of the sample preparation was used to improve the TEM lamella quality and reduce the Ga deposition in the surface. Certain precautions were taken to reduce the TEM sample oxidation. It was prepared just before the TEM study and transferred into the microscope as quickly as possible (usually in about 40–60 s). TEM studies were carried out on a FEI Titan 80–300 aberration corrected transmission electron microscope. EF TEM images were recorded using the Tridium 863 imaging filter (Gatan Inc). EEL spectra were acquired in STEM mode in the energy loss range 490–1100 eV to determine local ratio of oxygen, iron and neodymium in the sample. Lorentz microscopy with a Fresnel mode was used to study the domain wall structure of the samples. Qualitative magnetic imaging was performed in zero magnetic field environment by turning the objective lens off. Low-magnification bright field (BF) scanning TEM (STEM) mode with a partially blocked diffraction disk by a dark field (DF) detector was used to visualize the magnetic domains. The exact position of the magnetic domain walls was detected in TEM Lorentz (Fresnel) mode.

3. Results

In Fig. 1 the BSE SEM micrograph of the studied NdFeB-based commercial alloy is shown. The size of $Nd_2Fe_{14}B$ grains is about 20–50 μm, and they appear dark in the BSE micrograph. Nd-rich phases are visible along the GBs and in GB TJs. Their grain size is about 3 to 10 μm. They have high Nd content and, therefore, brighter contrast in BSE. This conclusion is also supported by the results of EDX analysis, which are listed in Table 1. The elemental composition in this table and in the following text is given in atomic percent. The bright areas in the TJs between $Nd_2Fe_{14}B$ grains contain high amount of oxygen. It is because the commercial NdFeB-based permanent magnets frequently contain a tangible amount of neodymium oxide Nd_2O_3 in TJs [13–20]. Can the $Nd_2Fe_{14}B$/$Nd_2Fe_{14}B$ GBs also contain oxygen? Using the analytical facilities in SEM, it is not possible to detect thin GB layers due to the limited spatial resolution. In this case, the TEM-based techniques are necessary to be used. We performed such detailed screening of our sample with simultaneous EELS elemental composition measurements for oxygen, neodymium and iron.

In Fig. 3a to e five high-angle annular dark field (HAADF) STEM micrographs are given showing five triple joints in our samples. These TJs contain bulk and GB phases with various composition. For the numbered areas, the content of iron, neodymium and oxygen was measured by EELS; the respective data are given in Table 2. For these areas, HR TEM study was not performed, therefore, the phase composition of the grains, TJs and GBs was estimated only by the corresponding concentration ratio.

Fig. 3a shows the junction of three grains of the $Nd_2Fe_{14}B$ phase (areas 3, 4 and 5). The phase in the TJ (area 1) contains practically no oxygen, as well as other regions in this micrograph. Area 1 contains neodymium and iron in approximately equal proportions. This composition does not fit to any of their binary or ternary phases and most likely the material in TJ is a mixture of Fe and Nd phases. The GB between areas 3 and 4 marked by an elongated rectangle 2 also contains a mixture of neodymium and iron, without oxygen, in a ratio of about 7:2.

In Fig. 3b the contact region between two grains of the $Nd_2Fe_{14}B$ phase is presented (areas 4 and 5). The analysis of the EELS data shows no traces of oxygen. The boundary between them (area 3) also does not contain oxygen, but there is approximately twice as much neodymium in it as in the volume of the $Nd_2Fe_{14}B$ grains. This means, most likely, that this GB contains pure neodymium. The TEM contrast varies a lot inside the TJ, which can indicate the variation in the local elemental composition. The results of the EELS analysis support this conclusion. Area 1, most likely, consists of iron and neodymium oxides, since it contains about 20% of oxygen, while area 2 consists of a mixture of neodymium and iron, having a higher contrast due to the higher specific weight.

In Fig. 3c four regions of different composition can be distinguished. First, these are the grains of the $Nd_2Fe_{14}B$ phase (areas 4 and 5). They do not contain oxygen at all, as in the previous figures. The boundary between them (area 3) consists of pure neodymium, with no signs of oxygen or iron. Area 2 is a grain of neodymium oxide, and at the border between this grain 2 and region 4 there is a wide strip 1 containing mixture of neodymium and neodymium oxide, which follows from the contrast in this region (compare the results for the areas 1 and 2 in Fig. 3e).

Fig. 3d shows a TJ formed by two grains of the $Nd_2Fe_{14}B$ phase (areas 4 and 5) and a grain of neodymium oxide Nd_2O_3 (area 2). The junction of these three grains (area 1) is filled with almost pure neodymium with a small admixture of iron. The boundary between the $Nd_2Fe_{14}B$ phase (grain 4) and neodymium oxide (grain 2), shown by dashed rectangle (area 3) contains a little oxygen, as well as iron and neodymium in a ratio of about 5:3.

The junction of two grains of the $Nd_2Fe_{14}B$ phase (areas 3 and 2) and grain of the Nd_2O_3 phase (area 4) is shown in Fig. 3e. The analysis shows almost the same neodymium content at the boundary between grains 3 and 2 as in the volume of $Nd_2Fe_{14}B$ grains, but a slightly reduced iron concentration and about 7% of oxygen. Apparently, this boundary contains neodymium oxide, similar to the boundaries shown below in Fig. 4.

It is important to mention when analyzing the elemental composition of GB phases, one have to take into account that in some cases the results can be affected by the material in neighboring grains, if the GB does not go parallel to the electron beam. Thus, the screening with EELS-based elemental analysis permitted to determine that some of Nd-rich layers in $Nd_2Fe_{14}B$/$Nd_2Fe_{14}B$ GBs contain not only neodymium and sometimes iron, but also oxygen. More detailed analysis of such GBs has been performed by means of EF TEM for the elemental distribution, HR TEM for crystalline lattice characterization, as well as of Lorentz microscopy for visualization of the local magnetic structure.

We considered in more details one individual GB junction point (see Fig. 4). In Fig. 4a the bright field TEM micrograph is given showing three grains of $Nd_2Fe_{14}B$ phase with three GBs and GB TJ in the middle. Elemental mapping of the same area was received by means of EFTEM (Fig. 4a) using the O K, Fe L and Nd M edges. Additionally, the elemental composition was measured for three different locations in STEM EELS mode. The results of the EELS quantification are given in Table 3. Inside the $Nd_2Fe_{14}B$ phase in the area A, the Nd/Fe ratio is close to 1:7, i.e. to the composition of stoichiometric $Nd_2Fe_{14}B$ compound. The area B inside the TJ appears in the micrograph almost blue. It contains a Nd-rich phase and consists of Nd with a certain amount of oxygen (see Table 3). The GBs (area C in Fig. 4b) are rather thin (about 10–15 nm) and have composition with even higher oxygen content close to that in the neodymium oxide, Nd_2O_3.

Though we tried to minimize the time when the sample was exposed to the air (40 to 60 s), some oxidation did take place. We can estimate the sample oxidation during its transfer from FIB to the TEM site by the oxygen content from $Nd_2Fe_{14}B$ phase area. This

Table 1
Results of the EDX spectra quantification for NdFeB-based commercial alloy: sample matrix (area 1 in Fig. 1) and GB TJ (area 2 in Fig. 1).

Element	Area 1	Area 2
O K	4.8	56.6
Nd L	10.	33.03
Fe K	81.4	4.2
Dy L	3.5	6.2

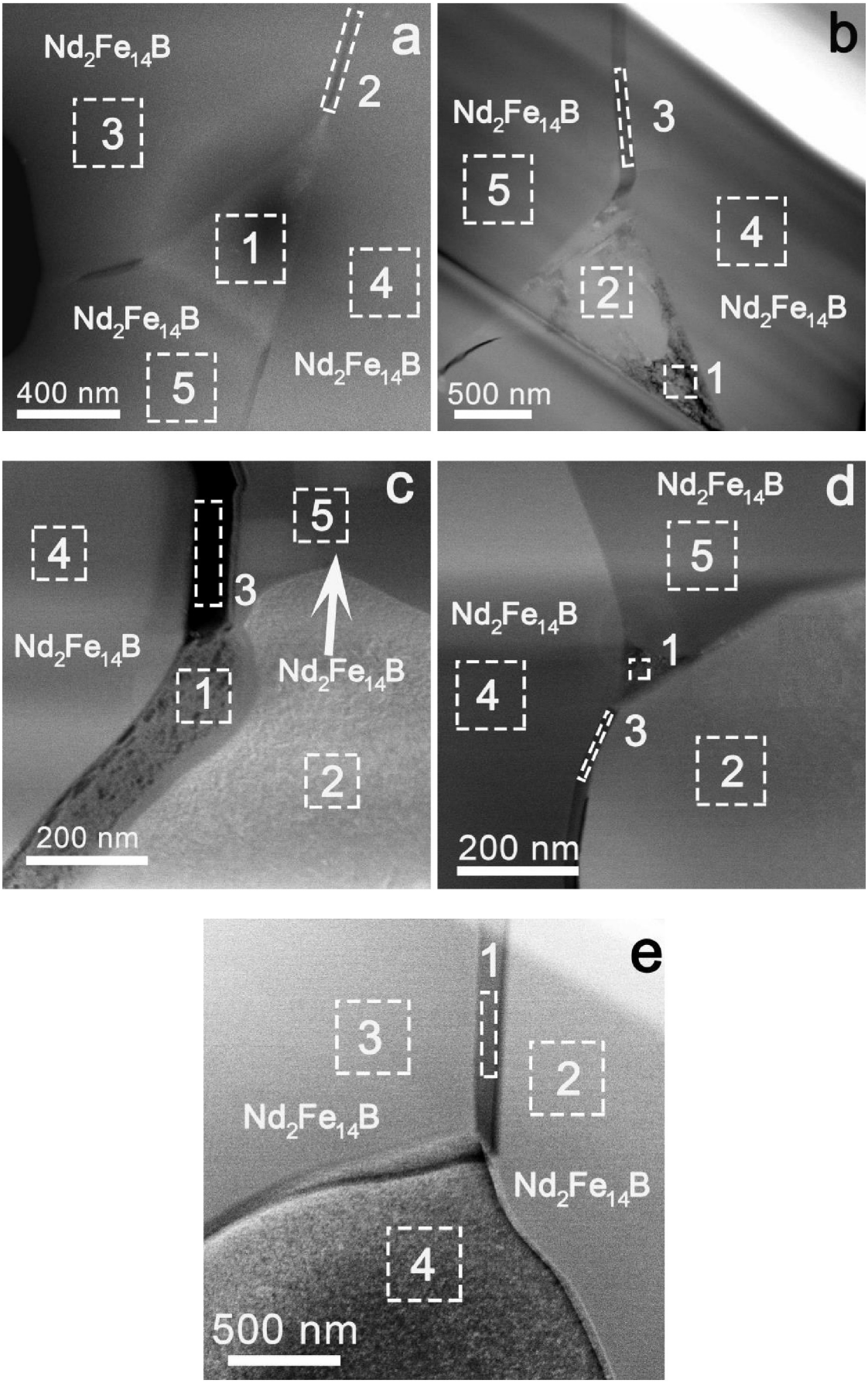

Fig. 3. HAADF STEM micrographs showing different triple joints containing various bulk and GB phases (see detailed escripition in the text). For numbered areas the compositions were measured by EELS, the respective data in at. % are given in Table 2.

Table 2
Results of the EELS spectra quantification for NdFeB-based commercial alloy, areas shown in Fig. 3.

Element	Area 1	Area 2	Area 3	Area 4	Area 5
Fig. #	Fig. 3a				
O K	4.2	0.0	1.1	2.4	0.0
Nd L	44.7	22.7	81.4	80.9	81.9
Fe K	51.1	77.3	17.5	16.7	18.1
Element	area 1	area 2	area 3	area 4	area 5
Fig. #	Fig. 3b				
O K	19.4	0.0	0.0	0.0	0.0
Nd L	63.6	65.0	37.6	17.3	15.3
Fe K	17.0	39.0	62.4	82.7	84.7
Element	area 1	area 2	area 3	area 4	
Fig. #	Fig. 3c Fig. 2c				
O K	9.27	19.28	0.0	0.0	0.0
Nd L	90.73	80.72	100	17.6	16.7
Fe K	0.0	0.0	0.0	82.4	83.3
Element	area 1	area 2	area 3	area 4	area 5
Fig. #	Fig. 3d Fig. 2d				
O K	0.0	34.56	4.2	14.2	0.0
Nd L	97.1	65.44	34.7	15.7	16.4
Fe K	2.9	0.0	51.1	84.3	83.6
Element	area 1	area 2	area 3	area 4	area 5
Fig. #	Fig. 3e				
O K	6.9	0.0	0.0	22.6	
Nd L	16.8	16.7	16.0	77.4	
Fe K	76.3	83.3	83.0	0.0	

phase does not contain oxygen, so the concentration of ~4% can be regarded as a reference value. It means that the oxides in GB and TJ phases are formed during the magnet manufacture, and not due the TEM sample oxidation.

Fig. 4c is the HR TEM micrograph from the area near GB layer (see the dashed square in Fig. 4a). Fig. 4d is the integrated radial intensity distribution versus scattering vector for the FFT patterns of the GB layer and from the area of TJ; the inserts are the corresponding FFTs. It follows from the plot in Fig. 4d that GB layer contains crystalline phase with cI80 cubic structure corresponding to Nd_2O_3 oxide, while the TJ consists of the mixture of Nd_2O_3 (cI80) and metallic Nd (hP4). Details on the phases crystal structure can be found in the next section in Table 4. Additionally, the 2D pattern belonging to hP4 metallic neodymium phase was indexed, see the bottom insert in Fig. 4d.

Fig. 5a shows the overview BF STEM magnetic image of the sample at zero field. It is easier to get an idea how the magnetic structure of the sample is arranged from this low magnification image. The opposite in-plane components of the magnetic field produce the dark and bright contrast in the magnetic domain, which are labeled and numbered from 1 to 7. The contrast switches at the domain walls, and domains appear like alternating brighter and darker parallel bands. The enlarged insert in Fig. 5b corresponds to the area of TEM and EF TEM images (see the dashed square in Fig. 5a). Fig. 5c is the Lorentz TEM image of the same area as Fig. 4b taken to show the exact location of the magnetic domain walls that are appeared as bright and dark lines. It is quite clear from the figure that the domain structure in $Nd_2Fe_{14}B$ grains is independent on that in the adjacent grains, and the magnetic domains are not visible inside the GB layers and TJ. This means that the magnetic domain walls are not connected across the GB layer. In other words, the GBs as well as TJ magnetically separate the domains in all three grains, and the GB Nd_2O_3 phase can serve for the magnetic decoupling of $Nd_2Fe_{14}B$ grains from each other, similar to that by the metallic Nd- rich GB layers [5,13].

Fig. 6 shows the TEM images of another area close to the TJ of three $Nd_2Fe_{14}B$ grains. In Fig. 6a the bright field TEM micrograph is given showing three grains of $Nd_2Fe_{14}B$ phase numbered as grains 1, 2 and 3 and GB TJ in the middle. Lines crossing the GBs and square 1 in TJ show the areas for HRTEM images. Fig. 6b shows the HRTEM image near the GB layer between $Nd_2Fe_{14}B$ grains 1 and 2. Fig. 6c shows the HRTEM image near the GB layer between $Nd_2Fe_{14}B$ grains 2 and 3. Fig. 6d shows the HRTEM image from the TJ area marked by the square 1 in (a). The fast Fourier transforms (FFT) in Figs. 6 e, f, g demonstrate that the GB layer between $Nd_2Fe_{14}B$ grains 1 and 2 as well as GB layer between $Nd_2Fe_{14}B$ grains 2 and 3 conatin the oxide Nd_2O_3. The FFT picture in Fig. 6g shows that for GB TJ contains the mixture of Nd (dotted red circles) and Nd_2O_3 (dotted blue circles).

4. Discussion

The oxides are almost inevitable in the NdFeB-based sintered permanent magnets [13–20]. In laboratory conditions, the special care is frequently taken to exclude the influence of oxygen [24]. These precautions are too expensive in case of industrial production, and oxygen is usually present in the sintered NdFeB-based permanent magnets [25]. X-ray diffraction (XRD) data show that they contain at least few percent of Nd_2O_3 or NdO_x phases with cI80 and fcc lattice, respectively [6,7,15,26,27]. Nd_2O_3 phase can also have hP5 hexagonal structure (for the reference of the Nd and neodymium oxides crystal structure see Table 4). Metallic Nd phase can exist either as a fcc or a double hcp (hP4) lattice. The oxide particles in $Nd_2Fe_{14}B$ grains TJs are clearly visible in SEM [5,6,13,14,16–19,28–30] and TEM [6,7,14,17,26,27,31,32]. In addition to the results obtained from XRD and electron diffraction, the EDS measurements also reveal the presence of oxygen in these non-metallic particles [7,15,16,20,28–30,33]. Thus, the bulk oxides are conventional in the sintered NdFeB-based permanent magnets and the overall oxygen content is far from negligible.

It is generally accepted that thin GB layers of non-ferromagnetic Nd-rich phase are responsible for the "magnetic isolation" or decoupling of $Nd_2Fe_{14}B$ grains from each other [4–13]. In turn, this magnetic isolation leads to high coercivity of the sintered NdFeB-based permanent magnets [5,6]. The question is whether these magnetically isolating Nd-rich GB layers always consist of metallic (or intermetallic) phase or they can also contain oxides?

Usually, the composition of GB layers in NdFeB-based permanent magnets is measured by EDS in TEM and SEM [6,39–41]. In these measurements, the content of main metallic elements is mostly determined [6,40], and only very seldom that of oxygen [6,39,41]. For example, the minima of iron and cobalt concentrations as well as maxima of oxygen, fluorine, neodymium and praseodymium concentrations were observed by EDS in the ~4 nm thin GB area [41]. Unfortunately, the data for oxygen concentration obtained by EDX are not very reliable in comparison with that for the metallic elements due to the low oxygen atomic mass, low peak-to-background ratio and overlapping EDX peaks. The EELS measurements of oxygen concentration are more accurate. However, only few works of this kind are available [22,23]. Zickler and co-authors observed $Nd_2Fe_{14}B/Nd_2Fe_{14}B$ GBs containing the 3–10 nm thin GB layers. EELS showed that these GB layers were depleted with Fe + Co and enriched with Pr + Nd and oxygen in comparison with bulk $Nd_2Fe_{14}B$ phase. Unfortunately, the analysis of phase composition of Pr–Nd–O-rich GB layers was lacking in the cited articles, as well as the evidence on $Nd_2Fe_{14}B$ phase magnetic decoupling.

Atom probe tomography was also applied to detect oxygen in NdFeB hard magnets [6,42]. The measured volume contained ~5 nm thin GB layer between $Nd_2Fe_{14}B$ grains. The grains expectedly contained iron, neodymium, praseodymium, boron and they were oxygen free. Contrary, the GB layer were free of boron and iron, but revealed the peak of oxygen and Nd + Pr mixture. Depending on the processing conditions, the GB phase was found to be either $Nd_6Fe_{13}Ga$ intermetallic compound, amorphous or crystalline neodymium oxide with cI80 structure. The amorphous Nd-rich GB layers were also observed in Refs. [5, 13, 40]. In Ref. [32] it was shown that the GB layer

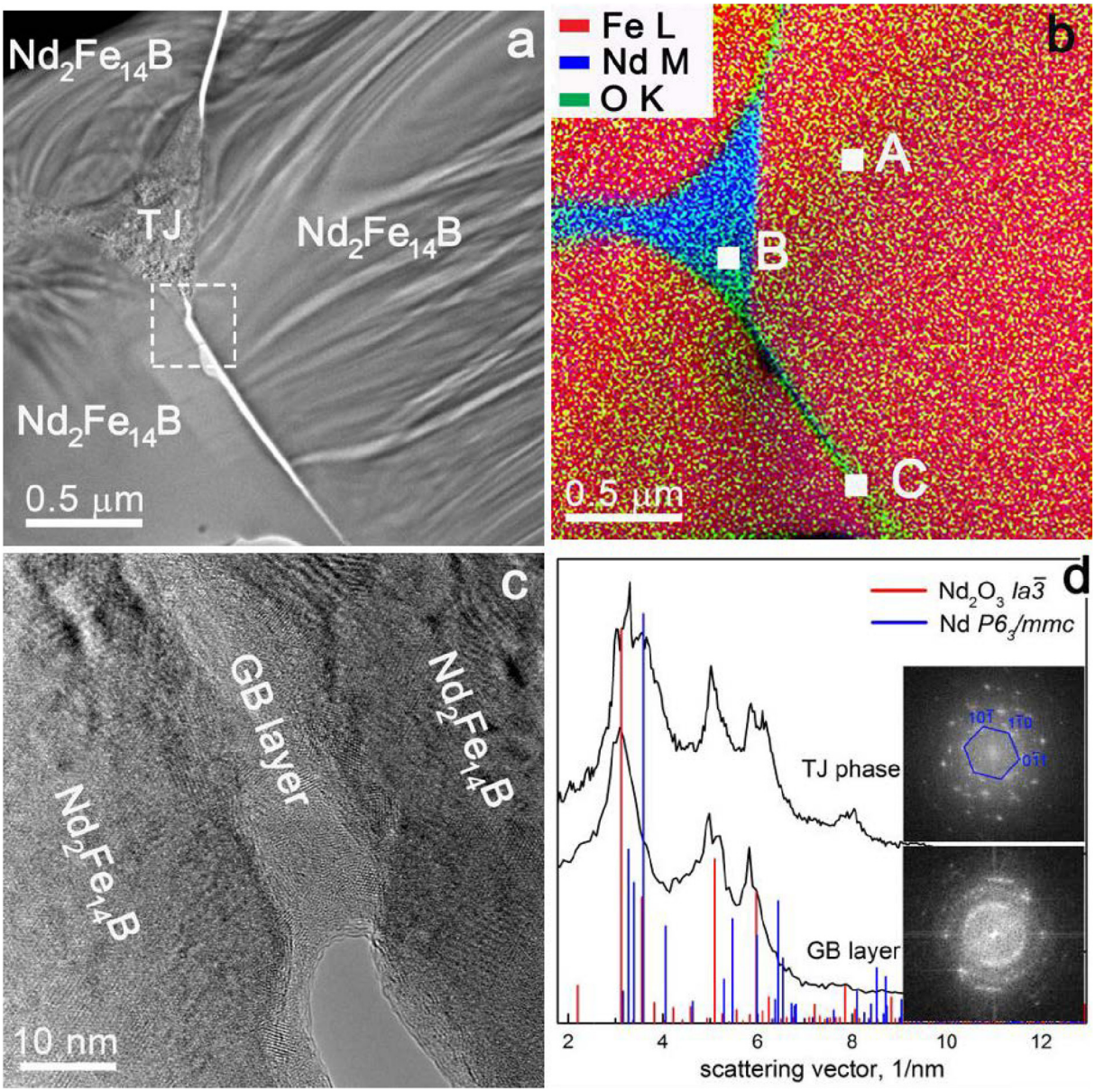

Fig. 4. TEM image of the area near the TJ of three $Nd_2Fe_{14}B$ grains (a) bright field TEM micrograph. (b) colored elemental map of the same area as in (a) constructed from the EFTEM images in Fe L, Nd M, and O K edge signals; the color code can be find in the insert; the elemental composition is given in Table 2. (c) HRTEM image near the GB layer between two $Nd_2Fe_{14}B$ grains from the area marked by dashed square in (a). (d) integrated radial intensity distribution versus scattering vector for the fast Fourier transforms (FFT) from the GB layer and TJ area (see the inserts); bar diagram shows the positions of the interplanar distances for Nd_2O_3 (cI80) and metallic Nd (hP4) phases; the bottom FFT from TJ contains the indexed 2D pattern of hP4 phase with the zone axis parallel to [111] direction.

Table 3
Result of EELS elemental composition measurements in the areas A, B and C in Fig. 4b, at. %.

Element	Area A	Area B	Area C
O K	4.2	10.4	63.1
Nd L	7.1	89.6	11.3
Fe K	88.7	0	26.6

phase composition depends on the content of trace alloying components.

In [27] the possible influence of GB phase on the magnetic properties of NdFeB alloys was analyzed based on the atomistic model and finite-element method simulation. The authors considered different GB phases, both metallic Nd (fcc and double hcp hP4) and neodymium oxides Nd_2O_3 (a-type, hP5 and c-type, cI80), and NdO (cF8). It was shown that some of these phases (namely, fcc Nd, Nd_2O_3 cI80 and NdO cF8) have less detrimental effect on $Nd_2Fe_{14}B$ grains coercivity.

Thus, summing up the published data we can assume that the presence of neodymium oxide is a characteristic feature of NdFeB-based magnets. For direct check of our hypothesis, we performed in this work the whole complex of experimental studies, namely the SEM, EDS, HRTEM, EFTEM, EELS, and Lorentz microscopy. SEM witnesses that oxide particles are indeed present in TJs of $Nd_2Fe_{14}B$ grains. EDS and EFTEM permitted to observe that some of Nd-rich GB layers contain not only neodymium, but oxygen as well. The STEM screening with EELS measurements of Nd, Fe and O content permitted to find such GBs with oxides among the "conventional" GBs with Nd-rich layers (Fig. 3). We

Table 4
Structural data for neodymium and oxide neodymium phases.

ICSD #	Space group symbol	Pearson symbol	Formula	Cell parameters	Ref.
100,211	$P6_3/mmc$	hP5	Nd_2O_3	a = 3.947 c = 6.277	[34]
100,216	$Im\bar{3}m$	cI5	Nd_2O_3	a = 4.41	[34]
191,535	$Ia\bar{3}$	cI80	Nd_2O_3	a = 11.08	[35]
	$Fm\bar{3}m$	cF8	NdO	a = 4.994	[35]
76,591	$Fm\bar{3}m$	cF4	Nd	a = 4.917	[36]
9,008,508	$P6_3/mmc$	hP2	Nd	a = 3.657 c = 5.9020	[37]
76,592	$P6_3/mmc$	hP4	Nd	a = 3.6582 c = 11.7966	[38]

do not conclude that GB phases of an oxide nature are unique or dominant in the structure of NdFeB-based permanent magnets. It is rather time consuming to make statistically significant conclusions on the share of such GBs in the structure of NdFeB-based permanent magnets by means of TEM. Such work devotes the special, separate study. Such work devotes the special, separate study. In our work, we demonstrate that oxide-based GB phases really exist in the NdFeB-based permanent magnet and they can good magnetically isolate the grains of $Nd_2Fe_{14}B$ phase.

The HRTEM images showed that such oxide GB layers are crystalline and have the lattice of neodymium oxide Nd_2O_3 rather than that of the metallic Nd or Nd-rich intermetallic compounds. Lorentz microscopy permitted to observe that the Nd_2O_3 GB layers prevent the migration of domain walls from one $Nd_2Fe_{14}B$ grain to another during remagnetization. Thus, the GB oxide layers are not only present among the Nd-rich GB ones, but they can indeed ensure the magnetic isolation between $Nd_2Fe_{14}B$ grains needed for high coercivity.

Thus, one can suppose that migration of domain walls and, therefore, the coercivity is controlled by the interphase boundaries between the bulk $Nd_2Fe_{14}B$ grains, on the one hand, and, on the other hand, (1) metallic Nd or Nd-rich intermetallic compounds in TJs; (2) metallic Nd or Nd-rich intermetallic compounds in GB layers; (3) Nd_2O_3 in TJs and (4) Nd_2O_3 in GB layers. During our experiments we investigated not only the locations shown in this paper but the rather big number of different areas in the samples. The collected statistics permits us to determine the specific area of interphase boundaries of classes (1) to (4), and to estimate in such a way semi-quantitatively their contribution to coercivity as (1):(2):(3):(4) ~ 2:1:5:2.

An important issue for the magnetic properties of NdFeB-based magnets is also the interplay between Nd-rich phase in TJs and Nd_2O_3 layers in GBs. The presence of thin films of Nd-rich phase(s) in the $Nd_2Fe_{14}B/Nd_2Fe_{14}B$ GBs is the special case of the more general phenomenon of intergranular thin films (IGFs) [43–60]. The IGFs can appear in equilibrium, non-equilibrium or steady-state structures [61–69]. In the majority of cases IGFs are tightly related to GB wetting, prewetting and premelting phase transformations (for review see [54,55] and references therein). The transformation between complete wetting (CW, Figs. 7c,d,g) and partial wetting (PW, Figs. 7a,b,g) of GBs was first predicted by Cahn [70], and Ebner and Saam [71] from the analysis of equilibrium in the region near the critical point of two-component phase diagram.

Recently an extremely interesting phenomenon of pseudo partial (or pseudo incomplete, or frustrated complete) GB wetting was predicted [72] and observed (see Figs. 7 e,f) [73]. This phase transition lies between the PW and CW and marked as PPW in the generic phase diagram proposed in [74] (Fig. 7g) [75–80]. In case of PPW, the thin GB layer (i.e. IGF) can contact the droplets (or particles) of a second phase at large non-zero contact angle (Fig. 7f) [80]. Such IGFs can be observed in the broad ranges of concentrations, temperature and/or pressure and drastically modify the properties of polycrystals. In contrast to the thick (usually several tens of nanometers) CW GBs, the PPW IGFs are only several nanometers thin and often difficult to be observed [78]. This kind of phase transition can take place not only during the liquid-phase sintering or annealing, but also during the mechanical treatment [77,81–84].

The transition from PW to CW of $Nd_2Fe_{14}B/Nd_2Fe_{14}B$ GBs in ternary NdFeB alloys takes place according to our data [85,86]. At 700 °C the fraction of completely wetted GBs is zero and it increases up to almost 100% at 1200 °C. The analysis of published data for the microstructure of liquid-phase sintered NdFeB-based multicomponent alloys shows that the amount of GBs with zero contact angle in these alloys is far below 100% [86]. In other words, during the typical liquid-phase sintering at ~1100 °C only low GB fraction is completely wetted. It means that the formation of thick Nd-rich phase IGFs during liquid-phase sintering by PW–CW phase transition is not the main reason for the appearance of a Nd-rich GB phase.

Later we observed that PPW GBs also exist in NdFeB alloys [79] and even make a significant fraction of the wetted GBs. We suppose that the PPW is responsible for the formation of magnetically separating Nd-rich IGFs for $Nd_2Fe_{14}B$ grains [87]. In this work we demonstrated that (i) the wetted IGFs in NdFeB-based alloys can contain not only metallic phases (as generally supposed for this material) but also the layers of neodymium oxide Nd_2O_3, and (ii) these layers can also effectively isolate the $Nd_2Fe_{14}B$ grains to increase the coercivity of NdFeB-based permanent magnets.

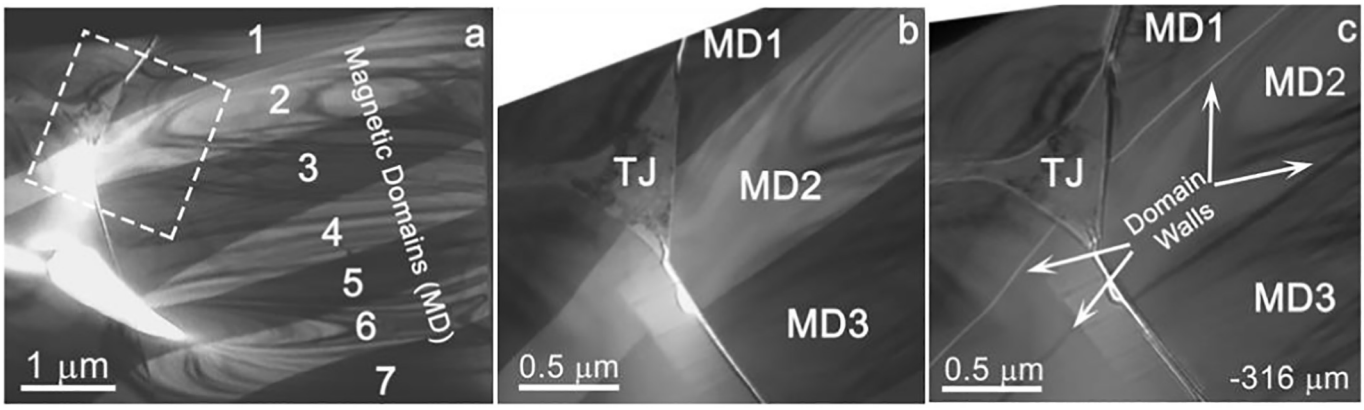

Fig. 5. TEM magnetic imaging of the sample at zero field. (a) Overview BF STEM image of the sample where magnetic domains marked by numbering. (b) Magnified dashed square region of the same area as Fig. 4a displaying the corresponding magnetic domains. (c) TEM Lorentz image of the area shown in (b) taken at the defocus of −316 μm representing the magnetic domain walls as bright and dark lines, marked by arrows, which are disrupted at the boundaries with TJ area. The image in (b) and (c) are rotated to coincide with the micrographs in Fig. 4.

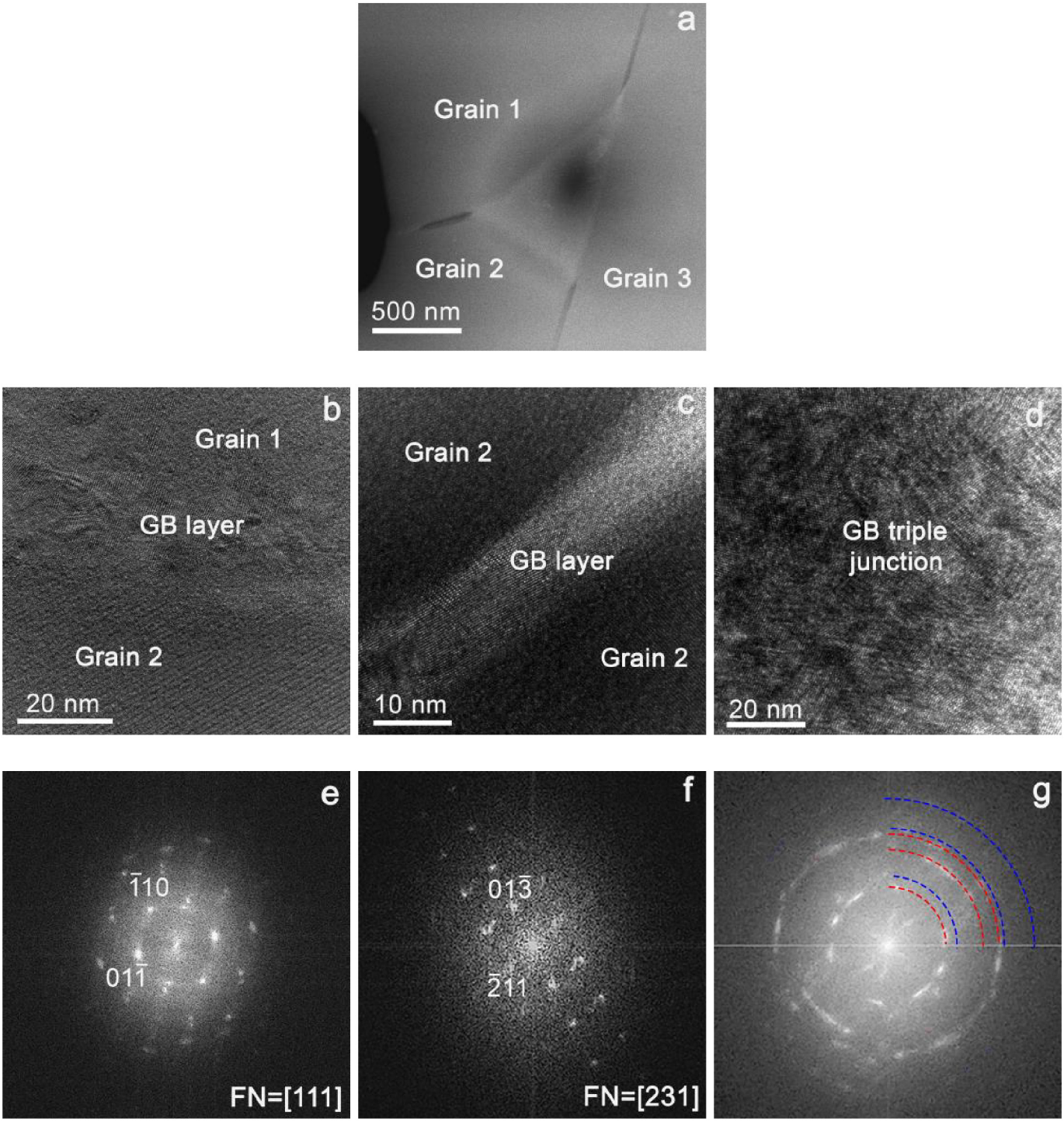

Fig. 6. TEM image of the area near the TJ of three $Nd_2Fe_{14}B$ grains 1, 2 and 3. (a) bright field TEM micrograph. Lines at GBs and square in TJ show the areas for HRTEM images. (b) HRTEM image near the GB layer between $Nd_2Fe_{14}B$ grains 1 and 2. (c) HRTEM image near the GB layer between $Nd_2Fe_{14}B$ grains 2 and 3. (d) HRTEM image from the TJ area marked by the square 1 in (a). (e, f, g) fast Fourier transforms (FFT) from the GB layers and TJ area (b, c, d) correspondingly. The GB layers in (e, f) contain Nd_2O_3. The TJ area (g) contains the mixture of Nd (dotted red circles) and Nd_2O_3 (dotted blue circles).

5. Conclusions

A certain fraction of GB layers of Nd-rich phase in the commercial NdFeB-based permanent magnets studied here contains oxygen. The crystalline lattice of these GB layers corresponds to that of the Nd_2O_3 and not to those of metallic Nd or Nd-rich intermetallic compounds. The Nd-oxide GB layers prevent the migration of domain walls from one $Nd_2Fe_{14}B$ grain to another during remagnetization. Thus, the GB oxide layers, similar to the "conventional" Nd-rich metallic ones, can ensure the magnetic isolation between $Nd_2Fe_{14}B$ grains needed for high coercivity. Therefore, the GB oxide layers can be used for further development of NdFeB-based permanent magnets in combination with GB layers containing the metallic Nd or intermetallic compounds.

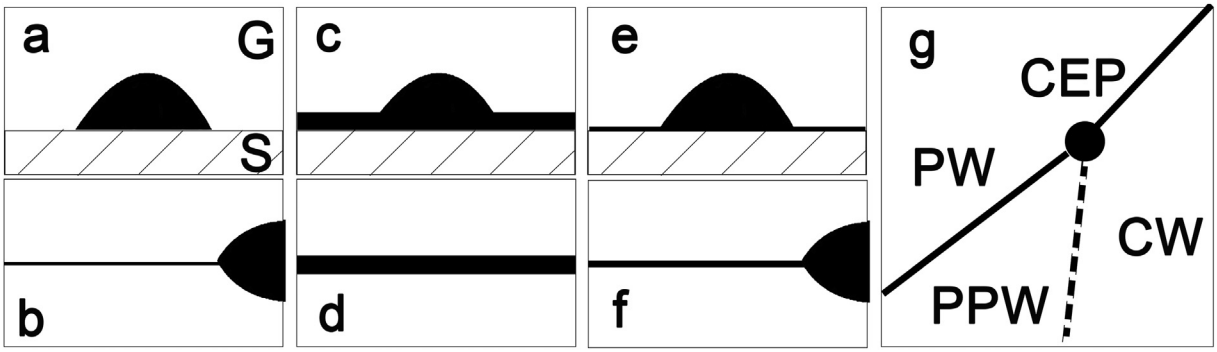

Fig. 7. The schemes for the wetting phase transitions of free surface and GB. (a) partial surface wetting, L – liquid phase, S – solid phase, G – gas phase; (b) partial GB wetting; (c) complete surface wetting; (d) complete GB wetting; (e) pseudopartial surface wetting; (f) pseudopartial GB wetting; (g) generic wetting phase diagram [71,73], PW – partial wetting, CW – complete wetting, PPW – pseudopartial wetting, CEP – critical end point, thick lines mark the discontinuous (first order) wetting transition, thin line mark the continuous (second order) wetting transition.

Data availability

The raw/processed data required to reproduce these findings cannot be shared at this time as the data also forms part of an ongoing study.

Author contribution

A. Mazilkin TEM measurements; B.B. Straumal results discussion, work planning; S.G. Protasova magnetic measurements; S. Gorji Lorentz microscopy; A.B. Straumal TEM measurements; M. Katter alloys preparation; G. Schütz results discussion; B. Barezky results discussion.

Declaration of Competing Interest

The authors declare that they have no known competing financial interests or personal relationships that could have appeared to influence the work reported in this paper.

Acknowledgements

This research was funded by the German Federal Ministry for Economic Affairs and Energy, based on the decision of German Bundestag, IGF grant number 19838 N. We thank Karlsruhe Nano Micro Facility (KNMF), a Helmholtz Research Infrastructure at Karlsruhe Institute of Technology (KIT) for the support of TEM study. The work was carried with partial support of the Scientific Facility Center at the Institute of Solid State Physics. The partial support of State Task of Russian Federal Ministry for Education and Science is acknowledged. S. Gorji acknowledges the Doctoral Scholarship provided by the DAAD. We also acknowledge support by the KIT-Publication Fund of the Karlsruhe Institute of Technology.

References

[1] M. Sagawa, S. Fujimura, N. Togawa, H. Yamamoto, Y. Matsuura, New material for permanent magnets on a base of Nd and Fe, J. Appl. Phys. 55 (1984) 2083–2087, https://doi.org/10.1063/1.333572.
[2] J.J. Croat, J.F. Herbst, R.W. Lee, F.E. Pinkerton, Pr–Fe and Nd–Fe-based materials: a new class of high-performance permanent magnets, J. Appl. Phys. 55 (1984) 2078–2082, https://doi.org/10.1063/1.333571.
[3] G.C. Hadjipanayis, R.C. Hazelton, K.R. Lawless, Cobalt-free permanent magnet materials based on iron-rare-earth alloys, J. Appl. Phys. 55 (1984) 2073–2077, https://doi.org/10.1063/1.333570.
[4] T. Helbig, K. Loewe, S. Sawatzki, M. Yi, B.-X. Xu, O. Gutfleisch, Experimental and computational analysis of magnetization reversal in (Nd,Dy)-Fe-B core shell sintered magnets, Acta Mater. 127 (2017) 498–504, https://doi.org/10.1016/j.actamat.2017.01.055.
[5] K. Hono, H. Sepehri-Amin, Strategy for high-coercivity Nd–Fe–B magnets, Scr. Mater. 67 (2012) 530–535, https://doi.org/10.1016/j.scriptamat.2012.06.038.
[6] T.T. Sasaki, Y. Takada, H. Okazaki, T. Ohkubo, T. Nakamura, T. Sato, A. Kato, Y. Kaneko, K. Hono, Role of Ga on the high coercivity of Nd-rich Ga-doped Nd-Fe-B sintered magnet, J. Alloys Compd. 790 (2019) 750–759, https://doi.org/10.1016/j.jallcom.2019.03.114.
[7] T.T. Sasaki, T. Ohkubo, Y. Takada, T. Sato, A. Kato, Y. Kaneko, K. Hono, Formation of non-ferromagnetic grain boundary phase in a Ga-doped Nd-rich Nd–Fe–B sintered magnet, Scr. Mater. 113 (2016) 218–221, https://doi.org/10.1016/j.scriptamat.2015.10.042.
[8] K.H.J. Buschow, Chapter 4 Magnetism and processing of permanent magnet materials, Handbook of Magnetic Materials 1997, pp. 463–593, https://doi.org/10.1016/S1567-2719(97)10008-7.
[9] H. Kronmüller, R. Fischer, M. Seeger, A. Zern, Micromagnetism and microstructure of hard magnetic materials, J. Phys. D. Appl. Phys. 29 (1996) 2274–2283, https://doi.org/10.1088/0022-3727/29/9/008.
[10] W. Rodewald, Rare-earth transition-metal magnets, Handbook of Magnetism and Advanced Magnetic Materials, John Wiley & Sons, Ltd, Chichester, UK, 2007https://doi.org/10.1002/9780470022184.hmm406.
[11] M. Seeger, J. Bauer, H. Kronmüller, J. Bernardi, J. Fidler, Magnetic and microstructural properties of sintered FeNdB-based magnets with Ga and Nb additions, J. Magn. Magn. Mater. 138 (1994) 294–300, https://doi.org/10.1016/0304-8853(94)90050-7.
[12] J. Bernardi, J. Fidler, M. Seeger, H. Kronmüller, Preparation and TEM-study of sintered $Nd_{18}Fe_{74}B_6Ga_1Nb_1$ magnets, IEEE Trans. Magn. 29 (1993) 2773–2775, https://doi.org/10.1109/20.281024.
[13] H. Sepehri-Amin, T. Ohkubo, T. Shima, K. Hono, Grain boundary and interface chemistry of an Nd–Fe–B-based sintered magnet, Acta Mater. 60 (2012) 819–830, https://doi.org/10.1016/j.actamat.2011.10.043.
[14] W.F. Li, T. Ohkubo, K. Hono, M. Sagawa, The origin of coercivity decrease in fine grained Nd–Fe–B sintered magnets, J. Magn. Magn. Mater. 321 (2009) 1100–1105, https://doi.org/10.1016/j.jmmm.2008.10.032.
[15] H. Okazaki, D. Billington, N. Tsuji, W. Ueno, Y. Kotani, S. Kawaguchi, K. Sugimoto, K. Toyoki, T. Fukagawa, T. Nishiuchi, K. Hono, S. Hirosawa, T. Nakamura, Quantitative identification of constituent phases in a Nd-Fe-B-Cu sintered magnet and temperature dependent change of electron density of $Nd_2Fe_{14}B$ studied by synchrotron X-ray diffraction, Acta Mater. 181 (2019) 530–536, https://doi.org/10.1016/j.actamat.2019.10.004.
[16] Z. Mural, L. Kollo, M. Xia, C.R.H. Bahl, A.B. Abrahamsen, H.N. Bez, J. Link, R. Veinthal, The effect of nano-TiC addition on sintered Nd-Fe-B permanent magnets, J. Magn. Magn. Mater. 429 (2017) 23–28, https://doi.org/10.1016/j.jmmm.2016.12.115.
[17] K. Lu, X. Bao, G. Chen, X. Mu, X. Zhang, X. Lv, Y. Ding, X. Gao, Coercivity enhancement of Nd-Fe-B sintered magnet by grain boundary diffusion process using Pr-Tb-Cu-Al alloys, J. Magn. Magn. Mater. 477 (2019) 237–243, https://doi.org/10.1016/j.jmmm.2019.01.062.
[18] W. Mo, L. Zhang, Q. Liu, A. Shan, J. Wu, M. Komuro, Dependence of the crystal structure of the Nd-rich phase on oxygen content in an Nd–Fe–B sintered magnet, Scr. Mater. 59 (2008) 179–182, https://doi.org/10.1016/j.scriptamat.2008.03.004.
[19] Y. Shinba, T.J. Konno, K. Ishikawa, K. Hiraga, M. Sagawa, Transmission electron microscopy study on Nd-rich phase and grain boundary structure of Nd–Fe–B sintered magnets, J. Appl. Phys. 97 (2005), 053504, https://doi.org/10.1063/1.1851017.
[20] E. Isotahdon, E. Huttunen-Saarivirta, V.-T. Kuokkala, Characterization of the microstructure and corrosion performance of Ce-alloyed Nd-Fe-B magnets, J. Alloys Compd. 692 (2017) 190–197, https://doi.org/10.1016/j.jallcom.2016.09.058.
[21] T.G. Woodcock, Y. Zhang, G. Hrkac, G. Ciuta, N.M. Dempsey, T. Schrefl, O. Gutfleisch, D. Givord, Understanding the microstructure and coercivity of high performance NdFeB-based magnets, Scr. Mater. 67 (2012) 536–541, https://doi.org/10.1016/j.scriptamat.2012.05.038.
[22] G.A. Zickler, J. Fidler, J. Bernardi, T. Schrefl, A. Asali, A combined TEM/STEM and micromagnetic study of the anisotropic nature of grain boundaries and coercivity in Nd-Fe-B magnets, Adv. Mater. Sci. Eng. 2017 (2017) 6412042, https://doi.org/10.1155/2017/6412042.
[23] G.A. Zickler, J. Fidler, Nanocompositional electron microscopic analysis and role of grain boundary phase of isotropically oriented Nd-Fe-B magnets, Adv. Mater. Sci. Eng. 2017 (2017) 1461835, https://doi.org/10.1155/2017/1461835.

[24] H. Sepehri-Amin, Y. Une, T. Ohkubo, K. Hono, M. Sagawa, Microstructure of fine-grained Nd–Fe–B sintered magnets with high coercivity, Scr. Mater. 65 (2011) 396–399, https://doi.org/10.1016/j.scriptamat.2011.05.006.

[25] X.D. Xu, T.T. Sasaki, J.N. Li, Z.J. Dong, H. Sepehri-Amin, T.H. Kim, T. Ohkubo, T. Schrefl, K. Hono, Microstructure of a Dy-free Nd-Fe-B sintered magnet with 2 T coercivity, Acta Mater. 156 (2018) 146–157, https://doi.org/10.1016/j.actamat.2018.06.037.

[26] T.-H. Kim, S.-R. Lee, S. Namkumg, T.-S. Jang, A study on the Nd-rich phase evolution in the Nd–Fe–B sintered magnet and its mechanism during post-sintering annealing, J. Alloys Compd. 537 (2012) 261–268, https://doi.org/10.1016/j.jallcom.2012.05.075.

[27] G. Hrkac, T.G. Woodcock, K.T. Butler, L. Saharan, M.T. Bryan, T. Schrefl, O. Gutfleisch, Impact of different Nd-rich crystal-phases on the coercivity of Nd–Fe–B grain ensembles, Scr. Mater. 70 (2014) 35–38, https://doi.org/10.1016/j.scriptamat.2013.08.029.

[28] F. Yang, L. Guo, P. Li, X. Zhao, Y. Sui, Z. Guo, X. Gao, Boundary structure modification and magnetic properties of Nd-Fe-B sintered magnets by co-doping with Dy_2O_3/S powders, J. Magn. Magn. Mater. 429 (2017) 117–123, https://doi.org/10.1016/j.jmmm.2017.01.029.

[29] Y. Wang, J. Ahn, D. Kim, W.J. Ren, W. Liu, Z.D. Zhang, C.J. Choi, Effect of washing process on the magnetic properties of Nd-Fe-B nanoparticles prepared by reduction-diffusion method, J. Magn. Magn. Mater. 439 (2017) 91–94, https://doi.org/10.1016/j.jmmm.2017.04.081.

[30] F. Chen, T. Zhang, W. Zhang, L. Zhang, Y. Jin, Dependence of the demagnetization behavior on the direction of grain boundary diffusion in sintered Nd-Fe-B magnets, J. Magn. Magn. Mater. 465 (2018) 392–398, https://doi.org/10.1016/j.jmmm.2018.06.023.

[31] G. Hrkac, K. Butler, T.G. Woodcock, L. Saharan, T. Schrefl, O. Gutfleisch, Modeling of Nd-oxide grain boundary phases in Nd-Fe-B sintered magnets, JOM. 66 (2014) 1138–1143, https://doi.org/10.1007/s11837-014-0980-5.

[32] T.-H. Kim, S.-R. Lee, J. Woo Kim, Y. Do Kim, H.-J. Kim, M.-W. Lee, T.-S. Jang, Optimization of the post-sintering annealing condition for the high Cu content Nd-Fe-B sintered magnet, J. Appl. Phys. 115 (2014), 17A770, https://doi.org/10.1063/1.4869157.

[33] M.-W. Lee, K.-H. Bae, S.-R. Lee, H.-J. Kim, T.-S. Jang, Microstructure and magnetic properties of NdFeB sintered magnets diffusion-treated with Cu/Al mixed DyCo alloy-powder, Arch. Metall. Mater. 62 (2017) 1263–1266, https://doi.org/10.1515/amm-2017-0189.

[34] P. Aldebert, J.P. Traverse, Etude par diffraction neutronique des structures de haute temperature de La_2O_3 et Nd_2O_3, Mater. Res. Bull. 14 (1979) 303–323, https://doi.org/10.1016/0025-5408(79)90095-3.

[35] C. Artini, M. Pani, J.R. Plaisier, G.A. Costa, Structural study of Nd oxidation by means of in-situ synchrotron X-ray diffraction (400≤T≤700°C), Solid State Ionics 257 (2014) 38–41, https://doi.org/10.1016/j.ssi.2014.01.034.

[36] G.J. Piermarini, C.E. Weir, Allotropy in some rare-earth metals at high pressures, Science. 144 (1964) 69–71, https://doi.org/10.1126/science.144.3614.69.

[37] R.W.G. Wyckoff, Crystal Structures - Volume 1, Interscience Publishers, New York, 1963https://doi.org/10.1107/S0365110X65000361.

[38] C. Lundin, A. Yamamoto, J. Nachman, Studies of solution ideality in the praseodymium-neodymium system, Acta Metall. 13 (1965) 149–154, https://doi.org/10.1016/0001-6160(65)90190-2.

[39] G. Ding, S. Guo, L. Chen, J. Di, J. Song, R. Chen, D. Lee, A. Yan, Coercivity enhancement in Dy-free sintered Nd-Fe-B magnets by effective structure optimization of grain boundaries, J. Alloys Compd. 735 (2018) 795–801, https://doi.org/10.1016/j.jallcom.2017.11.115.

[40] H. Sepehri-Amin, T. Ohkubo, S. Nagashima, M. Yano, T. Shoji, A. Kato, T. Schrefl, K. Hono, High-coercivity ultrafine-grained anisotropic Nd–Fe–B magnets processed by hot deformation and the Nd–Cu grain boundary diffusion process, Acta Mater. 61 (2013) 6622–6634, https://doi.org/10.1016/j.actamat.2013.07.049.

[41] F. Bittner, T.G. Woodcock, L. Schultz, C. Schwöbel, O. Gutfleisch, G.A. Zickler, J. Fidler, K. Üstüner, M. Katter, Normal and abnormal grain growth in fine-grained Nd-Fe-B sintered magnets prepared from He jet milled powders, J. Magn. Magn. Mater. 426 (2017) 698–707, https://doi.org/10.1016/j.jmmm.2016.10.139.

[42] K. Niitsu, A. Sato, T.T. Sasaki, R. Sawada, Y. Cho, Y. Takada, T. Sato, Y. Kaneko, A. Kato, T. Ohkubo, D. Shindo, K. Hono, Y. Murakami, Magnetization measurements for grain boundary phases in Ga-doped Nd-Fe-B sintered magnet, J. Alloys Compd. 752 (2018) 220–230, https://doi.org/10.1016/j.jallcom.2018.04.055.

[43] B.B. Straumal, A.A. Mazilkin, B. Baretzky, Grain boundary complexions and pseudopartial wetting, Curr. Opin. Solid State Mater. Sci. 20 (2016) 247–256, https://doi.org/10.1016/j.cossms.2016.05.006.

[44] J.G. Dash, H. Fu, J.S. Wettlaufer, The premelting of ice and its environmental consequences, Rep. Prog. Phys. 58 (1995) 115–167, https://doi.org/10.1088/0034-4885/58/1/003.

[45] M. Kuzmina, M. Herbig, D. Ponge, S. Sandlöbes, D. Raabe, Linear complexions: confined chemical and structural states at dislocations, Science. 349 (2015) 1080–1083, https://doi.org/10.1126/science.aab2633.

[46] P.R. Cantwell, M. Tang, S.J. Dillon, J. Luo, G.S. Rohrer, M.P. Harmer, Grain boundary complexions, Acta Mater. 62 (2014) 1–48, https://doi.org/10.1016/j.actamat.2013.07.037.

[47] W.D. Kaplan, D. Chatain, P. Wynblatt, W.C. Carter, A review of wetting versus adsorption, complexions, and related phenomena: the Rosetta stone of wetting, J. Mater. Sci. 48 (2013) 5681–5717, https://doi.org/10.1007/s10853-013-7462-y.

[48] P.R. Bueno, J.A. Varela, E. Longo, SnO_2, ZnO and related polycrystalline compound semiconductors: an overview and review on the voltage-dependent resistance (non-ohmic) feature, J. Eur. Ceram. Soc. 28 (2008) 505–529, https://doi.org/10.1016/j.jeurceramsoc.2007.06.011.

[49] J. Luo, Y.-M. Chiang, R.M. Cannon, Nanometer-thick surficial films in oxides as a case of prewetting, Langmuir. 21 (2005) 7358–7365, https://doi.org/10.1021/la0505420.

[50] J. Luo, M. Tang, R.M. Cannon, W.C. Carter, Y.-M. Chiang, Pressure-balance and diffuse-interface models for surficial amorphous films, Mater. Sci. Eng. A 422 (2006) 19–28, https://doi.org/10.1016/j.msea.2006.01.001.

[51] D.R. Clarke, On the equilibrium thickness of intergranular glass phases in ceramic materials, J. Am. Ceram. Soc. 70 (1987) 15–22, https://doi.org/10.1111/j.1151-2916.1987.tb04846.x.

[52] J. Luo, Stabilization of nanoscale quasi-liquid interfacial films in inorganic materials: a review and critical assessment, Crit. Rev. Solid State Mater. Sci. 32 (2007) 67–109, https://doi.org/10.1080/10408430701364388.

[53] J. Luo, Y.-M. Chiang, Wetting and prewetting on ceramic surfaces, Annu. Rev. Mater. Res. 38 (2008) 227–249, https://doi.org/10.1146/annurev.matsci.38.060407.132431.

[54] A. Subramaniam, C.T. Koch, R.M. Cannon, M. Rühle, Intergranular glassy films: an overview, Mater. Sci. Eng. A 422 (2006) 3–18, https://doi.org/10.1016/j.msea.2006.01.004.

[55] I. MacLaren, Imaging and thickness measurement of amorphous intergranular films using TEM, Ultramicroscopy. 99 (2004) 103–113, https://doi.org/10.1016/j.ultramic.2003.10.002.

[56] S.J. Dillon, M. Tang, W.C. Carter, M.P. Harmer, Complexion: a new concept for kinetic engineering in materials science, Acta Mater. 55 (2007) 6208–6218, https://doi.org/10.1016/j.actamat.2007.07.029.

[57] M.P. Harmer, Interfacial kinetic engineering: how far have we come since Kingery's inaugural Sosman address? J. Am. Ceram. Soc. 93 (2010) 301–317, https://doi.org/10.1111/j.1551-2916.2009.03545.x.

[58] S.G. Protasova, B.B. Straumal, A.A. Mazilkin, S.V. Stakhanova, P.B. Straumal, B. Baretzky, Increase of Fe solubility in ZnO induced by the grain boundary adsorption, J. Mater. Sci. 49 (2014) 4490–4498, https://doi.org/10.1007/s10853-014-8146-y.

[59] N. Zhou, J. Luo, Developing grain boundary diagrams for multicomponent alloys, Acta Mater. 91 (2015) 202–216, https://doi.org/10.1016/j.actamat.2015.03.013.

[60] J. Luo, H. Cheng, K.M. Asl, C.J. Kiely, M.P. Harmer, The role of a bilayer interfacial phase on liquid metal embrittlement, Science. 333 (2011) 1730–1733, https://doi.org/10.1126/science.1208774.

[61] E.L. Maksimova, L.S. Shvindlerman, B.B. Straumal, Transformation of Σ17 special tilt boundaries to general boundaries in tin, Acta Metall. 36 (1988) 1573–1583, https://doi.org/10.1016/0001-6160(88)90225-8.

[62] L.S. Chang, B.B. Straumal, E. Rabkin, W. Gust, F. Sommer, The solidus line of the Cu-Bi phase diagram, J. Phase Equilibria. 18 (1997) 128–135, https://doi.org/10.1007/BF02665694.

[63] O.I. Noskovich, E.I. Rabkin, V.N. Semenov, B.B. Straumal, L.S. Shvindlerman, Wetting and premelting phase transitions in 38°[100] tilt grain boundary in (Fe-12 at.% Si)-Zn alloy in the vicinity of the A2-B2 bulk ordering in Fe-12 at.% Si alloy, Acta Metall. Mater. 39 (1991) 3091–3098, https://doi.org/10.1016/0956-7151(91)90042-Y.

[64] B. Straumal, O. Noskovich, V. Semenov, L. Shvindlerman, W. Gust, B. Predel, Premelting transition on 38°⟨110⟩ tilt grain boundaries in (Fe-10 at.% Si)-Zn alloys, Acta Metall. Mater. 40 (1992) 795–801, https://doi.org/10.1016/0956-7151(92)90021-6.

[65] R. Valiev, M.Y. Murashkin, B.B. Straumal, Enhanced ductility in ultrafine-grained Al alloys produced by SPD techniques, Mater. Sci. Forum 633–634 (2009) 321–332, https://doi.org/10.4028/www.scientific.net/MSF.633-634.321.

[66] N.Q. Chinh, T. Csanádi, J. Gubicza, R. Valiev, B. Straumal, T.G. Langdon, The effect of grain boundary sliding and strain rate sensitivity on the ductility of ultrafine-grained materials, Mater. Sci. Forum 667–669 (2010) 677–682, https://doi.org/10.4028/www.scientific.net/MSF.667-669.677.

[67] W. Rheinheimer, M.J. Hoffmann, Non-Arrhenius behavior of grain growth in strontium titanate: new evidence for a structural transition of grain boundaries, Scr. Mater. 101 (2015) 68–71, https://doi.org/10.1016/j.scriptamat.2015.01.021.

[68] A.K. Lawrence, A. Kundu, M.P. Harmer, C. Compson, J. Atria, M. Spreij, Influence of complexion transitions on microstructure evolution in specialty aluminas, J. Am. Ceram. Soc. 98 (2015) 1347–1355, https://doi.org/10.1111/jace.13421.

[69] L.S. Chang, E. Rabkin, B.B. Straumal, S. Hofmann, B. Baretzky, W. Gust, Grain boundary segregation in the Cu-Bi system, Defect Diffus. Forum. 156 (1998) 135–146, https://doi.org/10.4028/www.scientific.net/DDF.156.135.

[70] J.W. Cahn, Critical point wetting, J. Chem. Phys. 66 (1977) 3667–3672, https://doi.org/10.1063/1.434402.

[71] C. Ebner, W.F. Saam, New phase-transition phenomena in thin argon films, Phys. Rev. Lett. 38 (1977) 1486–1489, https://doi.org/10.1103/PhysRevLett.38.1486.

[72] F. Brochard-Wyart, J.M. Di Meglio, D. Quere, P.G. De Gennes, Spreading of nonvolatile liquids in a continuum picture, Langmuir. 7 (1991) 335–338, https://doi.org/10.1021/la00050a023.

[73] D. Bonn, J. Eggers, J. Indekeu, J. Meunier, E. Rolley, Wetting and spreading, Rev. Mod. Phys. 81 (2009) 739–805, https://doi.org/10.1103/RevModPhys.81.739.

[74] S. Rafaï, D. Bonn, E. Bertrand, J. Meunier, V.C. Weiss, J.O. Indekeu, Long-range critical wetting: observation of a critical end point, Phys. Rev. Lett. 92 (2004) 245701–245704, https://doi.org/10.1103/PhysRevLett.92.245701.

[75] J. Moon, P. Wynblatt, S. Garoff, R. Suter, Diffusion kinetics of bi and Pb–bi monolayer precursing films on cu (111), Surf. Sci. 559 (2004) 149–157, https://doi.org/10.1016/j.susc.2004.04.018.

[76] B.B. Straumal, X. Sauvage, B. Baretzky, A.A. Mazilkin, R.Z. Valiev, Grain boundary films in Al–Zn alloys after high pressure torsion, Scr. Mater. 70 (2014) 59–62, https://doi.org/10.1016/j.scriptamat.2013.09.019.

[77] B.B. Straumal, A.A. Mazilkin, X. Sauvage, R.Z. Valiev, A.B. Straumal, A.M. Gusak, Pseudopartial wetting of grain boundaries in severely deformed Al-Zn alloys, Russ. J. Non-Ferrous Met. 56 (2015) 44–51, https://doi.org/10.3103/S1067821215010198.

[78] B.B. Straumal, I. Konyashin, B. Ries, A.B. Straumal, A.A. Mazilkin, K.I. Kolesnikova, A.M. Gusak, B. Baretzky, Pseudopartial wetting of WC/WC grain boundaries in cemented carbides, Mater. Lett. 147 (2015) 105–108, https://doi.org/10.1016/j.matlet.2015.02.029.

[79] B.B. Straumal, A.A. Mazilkin, S.G. Protasova, A.M. Gusak, M.F. Bulatov, A.B. Straumal, B. Baretzky, Grain boundary phenomena in NdFeB-based hard magnetic alloys, Rev. Adv. Mater. Sci. 38 (2014) 17–28, https://doi.org/10.1515/rams-2014-38-0003.

[80] B.B. Straumal, A.O. Rodin, A.E. Shotanov, A.B. Straumal, O.A. Kogtenkova, B. Baretzky, Pseudopartial grain boundary wetting: key to the thin intergranular layers, Defect Diffus. Forum. 333 (2013) 175–192, https://doi.org/10.4028/www.scientific.net/DDF.333.175.

[81] B.B. Straumal, A.A. Mazilkin, S.G. Protasova, D.V. Gunderov, G.A. López, B. Baretzky, Amorphization of crystalline phases in the Nd–Fe–B alloy driven by the high-pressure torsion, Mater. Lett. 161 (2015) 735–739, https://doi.org/10.1016/J.MATLET.2015.09.076.

[82] X. Sauvage, M.Y. Murashkin, B.B. Straumal, E.V. Bobruk, R.Z. Valiev, Ultrafine grained structures resulting from SPD-induced phase transformation in Al-Zn alloys, Adv. Eng. Mater. 17 (2015) 1821–1827, https://doi.org/10.1002/adem.201500151.

[83] N.Q. Chinh, R.Z. Valiev, X. Sauvage, G. Varga, K. Havancsák, M. Kawasaki, B.B. Straumal, T.G. Langdon, Grain boundary phenomena in an ultrafine-grained Al-Zn alloy with improved mechanical dehavior for micro-devices, Adv. Eng. Mater. 16 (2014) 1000–1009, https://doi.org/10.1002/adem.201300450.

[84] B.B. Straumal, A.A. Mazilkin, S.G. Protasova, G. Schütz, A.B. Straumal, B. Baretzky, Observation of pseudopartial grain boundary wetting in the NdFeB-based alloy, J. Mater. Eng. Perform. 25 (2016) 3303–3309, https://doi.org/10.1007/s11665-015-1872-8.

[85] B.B. Straumal, Y.O. Kucheev, I.L. Yatskovskaya, I.V. Mogilnikova, G. Schutz, A.N. Nekrasov, B. Baretzky, Grain boundary wetting in the NdFeB-based hard magnetic alloys, J. Mater. Sci. 47 (2012) 8352–8359, https://doi.org/10.1007/s10853-012-6618-5.

[86] Y.O. Kucheev, A.B. Straumal, I.V. Mogil'nikova, B.B. Straumal, A.M. Gusak, B. Baretzky, Wetting of grain boundaries in hard-magnetic Nd-Fe-B alloys, Russ. J. Non-Ferrous Met. 53 (2012) 450–456, https://doi.org/10.3103/S106782121206003X.

[87] A. Mazilkin, B. Straumal, S. Protasova, B. Baretzky, Grain boundary wetting in the Nd–Fe–B-based alloy, Defect Diffus. Forum 380 (2017) 173–180, https://doi.org/10.4028/www.scientific.net/DDF.380.173.